

Development of a multiple input power conversion system for the DeciZebro

Bachelor Graduation project thesis

Thies de Boer (4513614)

Calvin Riekerk (4467450)

Technische Universiteit Delft



ABSTRACT

The DeciZebro is a six-legged autonomous robot is being developed by the Zebro team at the TU Delft. The robot should become autonomous and be able to "feed" itself like a real animal. Currently, it is only possible to charge the DeciZebro using a laptop charger. The goal is to allow the robot to charge itself without human intervention using a solar panel and a wireless charging pad. This thesis is part of a project that needs to develop a power management system and a battery management system that make it possible to charge the batteries wirelessly and by using a solar panel that will be placed on top of the DeciZebro. This thesis focuses on the design choices of the part of the project that handles the laptop charger, wireless charger and solar charger interfaces and the power converters necessary to supplement them.

The wireless charging interface was made in compliance with the Qi standard and allows for charging the batteries in conjunction with any Qi compliant wireless charging pad. Because a power path selector was built, the wireless charging receiver and the laptop charger could be implemented using a single Ćuk converter to regulate the voltage.

The solar panel voltage was also regulated using a Ćuk converter. This converter was designed with all the peripherals needed to implement a Perturb and Observe maximum power tracking algorithm for the solar panel.

Working prototypes have been produced for the solar panel Ćuk converter and for the power path selector. At the time of writing the wireless charging receiver has not yet been tested and the Ćuk converter for the laptop and wireless charger needs more testing to guarantee its successful implementation.

PREFACE

This thesis is part of the Bachelor Graduation Project in Electrical Engineering from the Delft University of Technology. The thesis describes one part of the development of an on-board power system for the DeciZebro which was proposed by Mattijs Otten of the Zebro team. It describes the design of the solar module, laptop charger and wireless power transfer interfaces with their necessary power converters. Chris Verhoeven was our supervisor and Daniël Booms our daily supervisor for this project.

Lastly we would like to thank the following people because this thesis would not be possible without their assistance and guidance:

Daniël Booms
Mattijs Otten
Chris Verhoeven
The Zebro Team

*Thies de Boer
Calvin Riekerk
Delft, June 18. 2018*

CONTENTS

1	Introduction	1
2	Program of requirements	2
3	System overview	3
3.1	Top level overview	3
3.2	Overview of the charging interfaces and conversion module	4
4	Photovoltaic module	6
4.1	Solar cell technologies	6
4.1.1	Polycrystalline Silicon	6
4.1.2	Monocrystalline Silicon	6
4.1.3	Thin film solar cells	6
4.2	Solar cell choice	7
5	Maximum power point tracking	8
5.1	Theoretical background	9
5.1.1	Constant voltage	9
5.1.2	Fractional open circuit voltage	9
5.1.3	Short circuit current method	9
5.1.4	Perturb and Observe	9
5.1.5	Incremental inductance	10
5.2	Design	11
6	Wireless Charging Module	13
6.1	Theoretical background	13
6.2	Qi	13
6.2.1	Communication with the transmitter	14
6.3	Design	15
6.3.1	Receiver coil	15
6.3.2	Dual resonant circuit	16
7	Power conversion	17
7.1	Theoretical background	17
7.1.1	The Ćuk converter in different states	17
7.2	Design	19
7.2.1	Power path controller	19
7.2.2	Ćuk converter of the laptop and Qi input	20
7.2.3	Ćuk converter of the solar module	21
7.2.4	Safety	21
8	Testing and results	22
8.1	Solar panel	22
8.2	Ćuk converter of the solar panel	23
8.3	Power path selector	24
8.4	Ćuk converter of the wireless charging module and the laptop charger	24
8.5	Cost analysis	25
8.5.1	Prototype	25
8.5.2	Semi-mass production	25

9	Conclusion and recommendations	26
9.1	Design process	26
9.2	Evaluation of sub-systems	26
9.3	Future work and recommendations.	26
A	Schematics and drawing	27
A.1	Main	27
A.2	Wireless power transfer	29
A.3	Power conversion	31
A.4	Drawing of the DeciZebro.	33
B	Derivations of the ripple current of the inductors and ripple voltage of the coupling capacitor from a \acute{C}uk converter	35
B.1	Ripple voltage of the coupling capacitor	35
B.2	Ripple current of the inductors	35
	Bibliography	36

1

INTRODUCTION

The DeciZebro is an autonomous six legged robot developed by the Zebro team of the TU Delft. The main goal of the Zebro team is to demonstrate swarm behaviour with their robots. To realize this goal the robots have to be autonomous which means that the robots should be able to make their own decisions and be able to carry out these decisions themselves.

The current power management system is only able to charge with a laptop charger. The power management system that needs to be developed should include a solar based charging module, a wireless power transfer system and a laptop charging interface. Additionally a new battery management system is required for this power management system.

The development of the power management system with battery management system was split between three subgroups. Each subgroup is responsible for one of the following:

1. The battery management system and output conversion of the power management system.
2. The input conversion of the power management system with the wireless power transfer module, solar module and laptop charging interface.
3. The control for the different modules of the power management system.

The subgroup of this thesis was responsible for the input conversion of the power management system with the wireless power transfer module, solar module and laptop charging interface.

In the current state of development the robots are only able to charge with a laptop charger which means the robots need help from a human. This would defeat the purpose of an autonomous robot if it is not capable to feed itself like a real animal. A possible solution is to equip the robot with a receiver for inductive charging. With this method the DeciZebro is able to locate the nearest Zebro charging station and charge itself.

However imagine a situation in which the DeciZebro does not have sufficient power left to walk to the nearest Zebro charging station then the robot will stop and needs to be picked up by someone to charge it. A possible solution would be to facilitate the DeciZebro with a solar panel. This way the DeciZebro is able to charge while it is walking around. This means that it might be possible for the robot to reach its destination before it runs completely out of power.

After the program of requirements in chapter 2 an overview of the power management system is given in chapter 3. Subsequently the solar module, maximum power point tracking, wireless power transfer and power transfer sub-modules are discussed in chapters 4 to 7. The test results are discussed in chapter 8. Finally a conclusion will be given with recommendations in chapter 9.

2

PROGRAM OF REQUIREMENTS

This is the program of requirements of the complete power management system with all of its interfaces. The requirements include maximum dimensions, functionality, costs and safety. The requirements with no high importance for our subgroup are grayed out.

- Functional requirements
 1. The system must support 230VAC charging via a laptop charging interface.
 2. The system must include the receiver side of an inductive charging interface.
 3. The system must be able to charge the batteries with a solar panel.
 4. The system must be able to power the DeciZebro directly with a solar panel.
 5. The power supply must be able to deliver 16V - 1A continuously, with a peak of 3A, fused without voltage regulation.
 6. The power supply must be able to deliver 5V - 1A, fused with voltage regulation.
 7. The power supply must be able to deliver 3.3V - 1A, fused with voltage regulation.
 8. The system should contain a damage protection system.
- Embedding requirements
 1. The PCB of the whole system must fit within its designated area of 143x41mm.
 2. The solar panel must not be larger than 13x13cm to fit on the roof of the DeciZebro.
 3. The receiver coil must be placed at the bottom of the DeciZebro in a circular area with diameter 8cm.
 4. The battery management PCB must fit within its designated area of 56.3x27mm.
 5. The batteries must fit within the allocated hatched area of the drawing in appendix [A.4](#).
- System requirements
 1. The wireless power transfer system must charge via the Qi inductive charging standard.
 2. The output voltage of the DC-DC conversion must be able to vary between the 12.0V-16.8V at the power bus.
- Production requirements
 1. The total cost of the whole power system should be kept below €100.-.
 2. The system should be easy to mass produce.

3

SYSTEM OVERVIEW

This chapter will begin by giving an overview of the whole power management system (PMS) and battery management system (BMS) that needs to be designed. Then, it will be discussed how the tasks of the three subgroups have been divided. After that, the chapter will narrow its scope and focus on the part of the system that will be discussed in this thesis: The charging interfaces and their corresponding power conversion stages.

3.1. TOP LEVEL OVERVIEW

Figure 3.1 shows a top level overview of the power management system and battery management system.

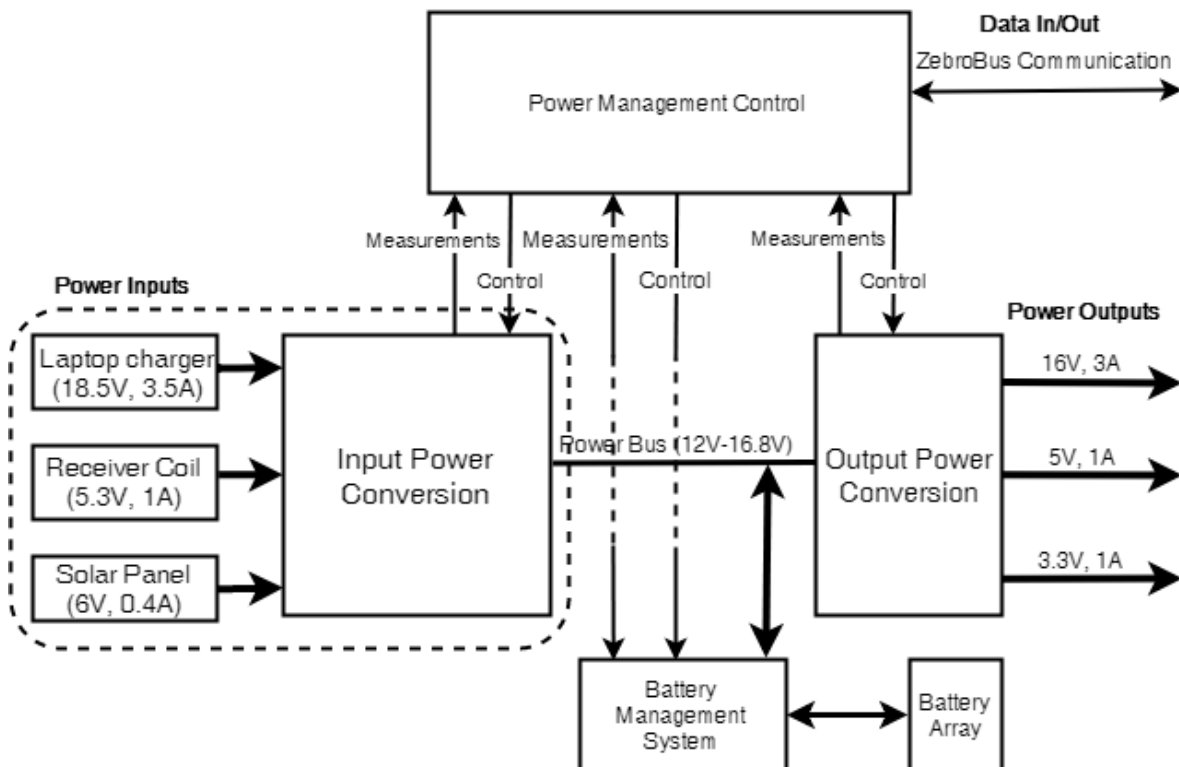


Figure 3.1: Top level overview of the power management system and the battery management system to be developed. Thin lines represent data signals while bold lines represent power signals.

For the project, the systems needed to be divided into three modules for the three subgroups. From the overview a certain separation in different modules becomes apparent and this was used in creating the subgroups and their tasks. The three subgroups and their responsibilities are:

1. Control subgroup. The tasks of the control subgroup include:
 - Ensuring safe operation of the PMS and BMS by measuring temperature, voltages and currents.
 - Communication with the main controller of the DeciZebro, using the ZebroBus protocol.
 - Offer control for each of the modules.
2. BMS and output subgroup. Their tasks include:
 - Select a battery type.
 - Design a battery management system.
 - Design output power converters.
3. The input subgroup. The tasks of this subgroup include:
 - Select a solar panel.
 - Select a receiver coil.
 - Design input power converters.

This thesis describes the activities and design choices of the input subgroup. Figure 3.1 shows a top level overview of the power management system and battery management system. From this figure it becomes more clear how the modules are related to one another. The part of the system enclosed by the dashed rounded rectangle will be discussed in this thesis.

3.2. OVERVIEW OF THE CHARGING INTERFACES AND CONVERSION MODULE

Now that an overview of the entire system has been given, this section will go into more detail on the different elements of the module that this thesis discusses. Figure 3.2 shows an overview of the system, but this time only with the parts and connections that are of relevance to our module.

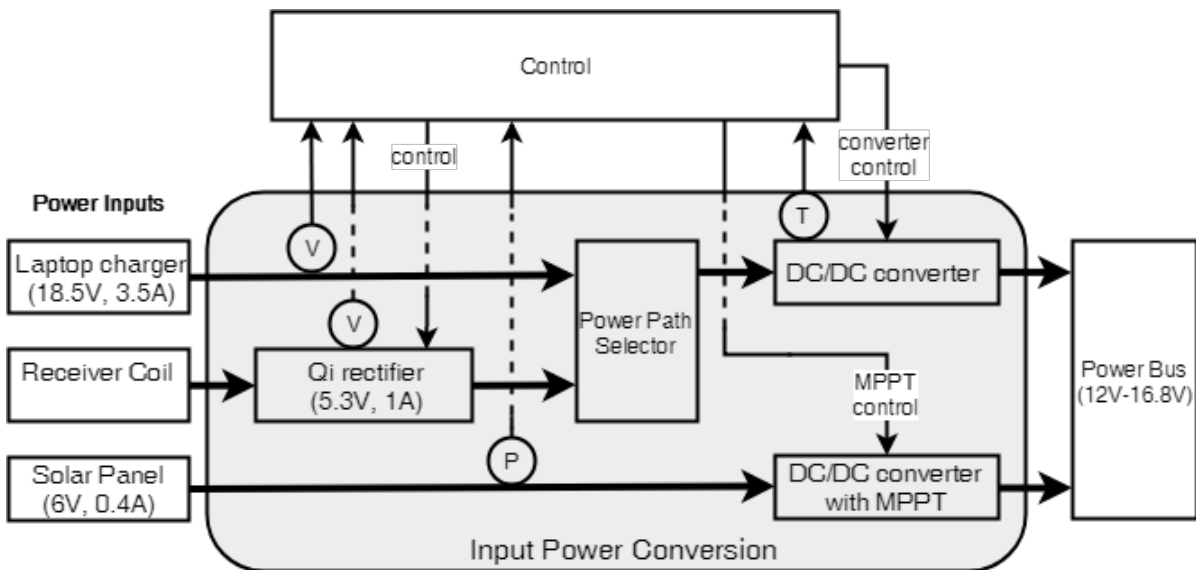


Figure 3.2: Overview of the charging interface and input power conversion part of the power management system. Thin lines represent data signals while bold lines represent power signals. 'T' represents a temperature measurement, 'V' represents a voltage measurement and 'P' represents a power measurement.

As a reference, the area with a grey background in the figure corresponds to the black box of 'Input Power Conversion' from figure 3.1. Here some smaller submodules have appeared. For each submodule the design choices will be discussed in the upcoming chapters of this thesis. The submodules and their role in the full design that will be discussed are:

- Solar panel: A solar panel needed to be placed on top of the DeciZebro. The design choices regarding the solar panel are discussed in chapter 4.

- DC/DC converter with MPPT for the solar panel: This converter needs to step up the voltage of the solar panel (around 6V) to the voltage at the power bus (12V-16.8V) and includes the tools to implement an MPPT method. The implementation of an MPPT method is discussed in chapter 5 and the DC/DC converter of the solar panel is discussed in chapter 7.
- Receiver coil with Qi compliant rectifier: A receiver coil needed to be selected for a wireless power transfer interface. The AC voltage from the coil needs to be converted into a DC voltage using a rectifier. Additionally the wireless power receiver needs to be Qi compliant. All of this will be discussed in chapter 6.
- Power Path Selector: The power path selector needs to connect the laptop charger or the wireless receiver module to a DC/DC converter depending on which charger is present. This will be discussed in chapter 7.
- DC/DC converter for the laptop charger and the wireless receiver module: This converter needs to change the voltage level of the laptop charger (typically 18.5V) or the wireless receiver module (typically 5.3V) to the voltage level of the power bus (12V-16.8V). This will also be discussed in chapter 7.

Furthermore, some measurements are done within the module. The voltage measurements at the laptop charger and wireless receiver interfaces allows the control subgroup to know whether a charger is present or not. The power measurement at the solar panel is needed for the control subgroup to implement an MPPT algorithm. Lastly, the temperature is measured at the DC/DC converter belonging to the laptop charger and wireless charging module to ensure the converter operates at a safe temperature.

4

PHOTOVOLTAIC MODULE

One of the requirements of the project is that the DeciZebro must be able to harvest solar energy by adding a solar panel on top of the robot. The benefits of this added solar panel are twofold: Firstly, by using energy from the solar panel during operation of the robot the battery depletes at a lower rate and the robot will be able to operate for a longer time without needing to be charged. Secondly, it enables the robot to become more autonomous. If the batteries are empty before the robot is able to reach a charging pad, it can still use the solar panel to charge its batteries to a level where it can bring itself to a nearby charging pad. This chapter includes a brief background on solar cell technologies and discusses our choices made on selecting a solar panel for the DeciZebro.

4.1. SOLAR CELL TECHNOLOGIES

Before choosing a solar panel, first a solar cell material needs to be chosen that is suitable for our project. This section will compare solar cell materials, focusing on two criteria that are important for our choice:

- The fraction of energy in the form of sunlight that can be converted via photovoltaics into electricity or the solar cell efficiency. Because a limited surface area is available to place a solar panel this efficiency needs to be high to take significant power from the solar panel.
- Price per Watt-peak. The design needs to be able to be mass produced, so very expensive solutions need to be avoided.

4.1.1. POLYCRYSTALLINE SILICON

The most widely used solar cells at the moment are polycrystalline silicon based cells, or poly-Si cells. These cells consist of multiple silicon crystals. Because the cells are so widely used, they are now cheap to produce compared to other solar cell technologies. Regardless of their low price, poly-Si can have reasonable conversion efficiencies: An efficiency of 22.4% was demonstrated by FhG-ISE under Standard Test Conditions (STC) [1]. The STC specify a cell temperature of 25°C and an irradiance of 1000 W/m² with an air mass 1.5. This standard is used to compare solar cells from different manufacturers.

4.1.2. MONOCRYSTALLINE SILICON

In contrast to poly-Si solar cells, monocrystalline silicon cells, or mono-Si cells, consist of only a single silicon crystal. As a result of this homogenous framework, they are more difficult to produce and thus more expensive than poly-Si solar cells. However, because of their structure they can reach conversion efficiencies much greater than poly-Si cells: Kaneka reported an efficiency of 26.7% for a monocrystalline silicon solar cell under STC.

4.1.3. THIN FILM SOLAR CELLS

Another solar cell technology that is currently available are thin film solar cells. Of the solar cells currently on the market, thin film cells generally have a lower conversion efficiency than c-Si solar cells, though progress in efficiency is coming with AIST reporting a laboratory cell efficiency of 21.0% for their CdTe solar cell [1]. The

advantage of thin film solar cells is the potential of this technology becoming very cheap. However, because currently c-Si solar cell technology is used much more widely, having over 85% of the PV market share [2], more research has been done into c-Si technologies. Consequently, the lower price for thin film solar cells in comparison to poly-Si cells is not quite to be seen on the market yet.

4.2. SOLAR CELL CHOICE

As stated in chapter 2, the whole power system for the DeciZebro should not cost more than €100 when mass produced. As a result, a solid middle ground between solar cell price and efficiency had to be looked for. This was found in poly-Si solar cells. These cells were chosen for their low price and their relatively high efficiency on the market. Another advantage is that poly-Si cells are very widely available on the market, so finding a replacement if the cells are out of stock should not be too difficult. The specific solar panel that was chosen is a 2.5 W solar panel with an operating voltage of about 6 V. The dimensions of the solar panel are 130 x 115 mm, so the solar panel should fit within its designated area of 130 x 130 mm as specified in chapter 2. According to the specifications as given by the manufacturer, the solar panel should hold a conversion efficiency of 16.7 %. The fact that the solar panel already has a relatively high operating voltage of 6 V is another advantage of the solar cell. Because of this the DC/DC converter, discussed in detail in chapter 7, that needs to bring the voltage of the solar panel to the voltage level of the power bus does not need to have a very high voltage gain. For applications requiring a large voltage gain, it becomes a problem to maintain a high conversion efficiency due to the high duty cycle needed [3].

5

MAXIMUM POWER POINT TRACKING

Figure 5.1 shows the typical I-V curve of a solar cell. It can be seen that by changing the operating voltage and current of a solar cell, the energy that is being generated by the solar cell changes tremendously. Under certain environmental conditions, one combination of voltage and current on the I-V curve results in the most power being taken from the cell. This point is called the maximum power point (MPP).

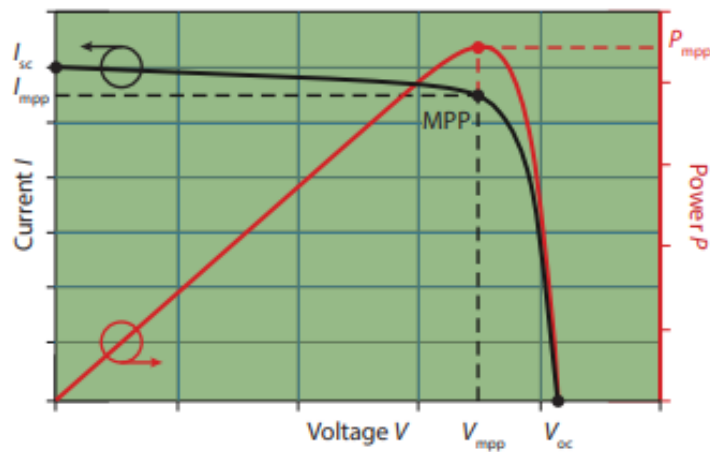


Figure 5.1: Typical Current-Voltage characteristics of a solar cell. The red curve shows the Power-Voltage characteristics. The open circuit voltage, the short circuit current and the maximum power point are indicated. [4]

This shows the importance of having some method to control the operating voltage and current of the solar panel. These methods are called maximum power point tracking (MPPT) techniques. Usually, MPPT methods are embedded in DC/DC converters. The voltage-current relationship of a solar panel depends on the load connected to it, which will usually cause the solar panel to work under sub-optimal operating conditions. Placing a DC/DC converter between the solar panel and the load with a certain voltage and current gain allows the solar panel to effectively have a different load connected to it, enabling it to deliver more energy.

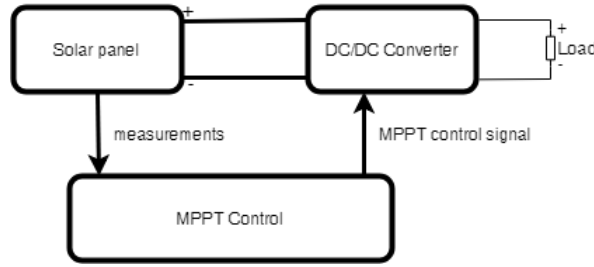


Figure 5.2: Overview of a solar panel connected to a DC/DC converter with MPPT ability.

These gains can be changed by controlling the duty cycle of the switch or switches of the DC/DC converter, which is done by a control subsystem. This control subsystem can set the duty cycle based on measurements taken, depending of the complexity of the MPPT technique used. An overview of a solar panel with MPPT implemented using a DC/DC converter can be found in figure 5.2. This chapter will list several MPPT methods and explains how these methods work. After this, the chapter will go on to cover what MPPT technique was chosen for our system, why this method was chosen and how this was implemented.

5.1. THEORETICAL BACKGROUND

5.1.1. CONSTANT VOLTAGE

For constant environmental conditions, the maximum power point voltage is always around the same value for a given solar panel. The constant voltage method exploits this by determining an optimal operating voltage given the environment the solar panel is in, and fixing the voltage at this value. This method is not an MPPT technique, because it does not actively change the operating voltage of the PV panel to seek a better operating point. Nonetheless, the method allows for reasonable results with a very small implementation complexity.

5.1.2. FRACTIONAL OPEN CIRCUIT VOLTAGE

The PV array voltage corresponding to the maximum power point exhibits a linear dependence with respect to the array open circuit voltage for different levels of irradiance and temperature [5]. This can be expressed by the following equation:

$$V_{mpp} = k_v * V_{oc} \quad (5.1)$$

where k_v is some constant of proportionality. The fractional open circuit voltage method works in a similar way to the constant voltage method, except that it now actively measures the open circuit voltage of a PV panel and determines the operating voltage as a fraction of this open circuit voltage using equation 5.1. This can be done by periodically disconnecting the load from the PV panel for a short time to measure and store its open circuit voltage and then reconnect the load again. After each measurement, the operating voltage can be adjusted based on the result.

5.1.3. SHORT CIRCUIT CURRENT METHOD

The short circuit current method works very much the same way as the fractional open circuit voltage method, with the difference being that now the PV current is looked at rather than the PV voltage. This method utilizes the fact that the optimal operating current of a PV cell is linearly proportional to the short circuit current or:

$$I_{mpp} = k_c * I_{sc} \quad (5.2)$$

where k_c is some constant of proportionality [6]. This relationship is used in the method proposed in [7] where a PV array is shorted periodically to measure its short circuit current and subsequently compute the operating current of the array using equation 5.2. An advantage of this method over fractional open circuit voltage that was observed in [7] was that k_c was shown to be much more consistent under different temperature and irradiance conditions than k_v .

5.1.4. PERTURB AND OBSERVE

The Perturb and Observe (P&O) algorithm is the most widely used MPPT method, because it has a good performance and is not difficult to implement. It works by periodically increasing or decreasing the PV voltage.

After changing the PV voltage, the power output of the solar panel is measured and compared to the power output before the change. If the power output has increased, the voltage will keep changing into the same direction. Alternatively, if the power output has decreased, it can be concluded that the solar panel is moving away from its maximum power point and the voltage will be changed in the opposite direction. A flow-chart that demonstrates the properties of the algorithm more clearly can be found in figure 5.3.

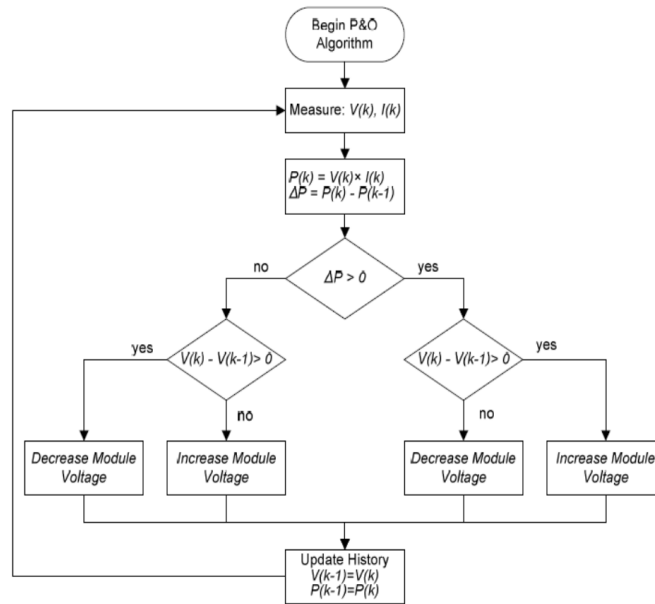


Figure 5.3: A flow chart taken from [8] that shows the working principles of the P&O algorithm.

In the P&O algorithm, this functionality results in the power output oscillating around the maximum power point, because the algorithm always keeps looking for a better point of operation. This effectively wastes some of the energy available. A converter can only switch at a finite number of duty cycles. Research from [9] uses this by showing that during steady state conditions, the power oscillation around the maximum power point is proportional to the step size of the duty cycle. Thus, by having small duty cycle steps the disadvantage of the P&O of energy losses during steady state operation can be partially overcome.

5.1.5. INCREMENTAL INDUCTANCE

The incremental inductance algorithm builds onto the P&O algorithm in the sense that it also changes the PV voltage and compares measurement samples to see how the solar panel power output reacts to the changes applied. However, the advantage of this algorithm is that it no longer has the problem of an oscillating power output. Following from the fact that dP/dV must be 0 at the maximum power point, it can be derived that at the maximum power point, $dI/dV + I/V = 0$ [10]. With this knowledge, an extra statement can be added to let the solar panel maintain its voltage once it has reached its maximum power point.

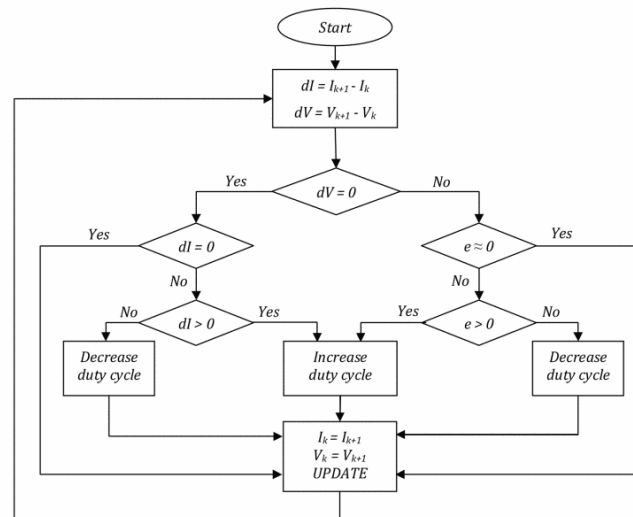


Figure 5.4: A flow chart taken from [10] that shows the working principles of the incremental conductance algorithm.

Figure 5.4 shows a flow chart of the incremental conductance MPPT method. Here e is the difference between the instantaneous conductance (I/V) and the incremental conductance (dI/dV) [10]. Because of this extra state, the performance of the incremental conductance method will be slightly higher than P&O, especially in situations with stable environmental conditions.

5.2. DESIGN

The P&O algorithm has a high performance but a relatively low complexity. Considering the DeciZebro will be moving around most of the time, it will rarely find itself in a situation with constant environmental and irradiance conditions. Consequently, the advantage of the incremental inductance method will be insignificant for our purpose. For this reason, the P&O MPPT method was chosen for the solar panel. The implementation consists of a power sensor, a Ćuk converter with a logic level MOSFET as a switch and a microcontroller to control this MOSFET. Using an algorithm similar to that of figure 5.3, the control subgroup implements the P&O algorithm on the microcontroller [11]. The design of the Ćuk converter with MPPT can be seen in figure 5.5.

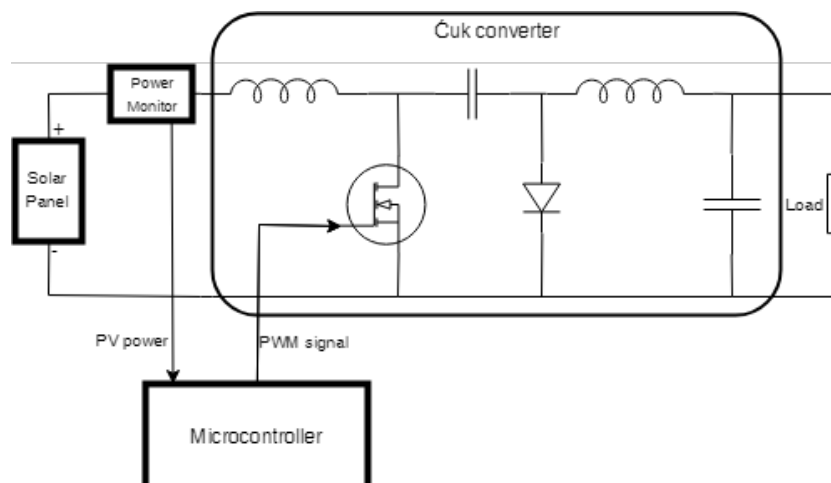


Figure 5.5: Schematic of the Ćuk converter with the necessary peripherals to implement the P&O algorithm.

The gate of the MOSFET receives a PWM signal with a certain duty cycle that is controlled by the microcontroller logic. For a Ćuk converter, the following relationship holds between the output voltage and the duty

cycle:

$$\frac{V_{out}}{V_{solar}} = -\frac{D}{1-D} \quad (5.3)$$

This equation can be rewritten to express the solar panel voltage as a function of the output voltage and the duty cycle:

$$V_{solar} = -V_{out} * \frac{1-D}{D} \quad (5.4)$$

As the DC/DC converter gets connected to the power bus, V_{out} simply becomes the power bus voltage. This means that the solar panel voltage can be controlled by adjusting the duty cycle with the microcontroller. The power sensor is used to measure the power coming out of the solar panel, this will be compared by the microcontroller with the power of a previous sample and the duty cycle will be increased or decreased accordingly.

6

WIRELESS CHARGING MODULE

In order to become more autonomous the DeciZebro needs to make use of a wireless charging module. This would give the DeciZebro the option to "feed" itself by going to one of the charging stations and leave when it is fully charged. This chapter will give a quick overview of how wireless power transfer works, some information about the Qi standard and how this was implemented in the power system.

6.1. THEORETICAL BACKGROUND

The general overview of a wireless power transfer system is given in figure 6.1.

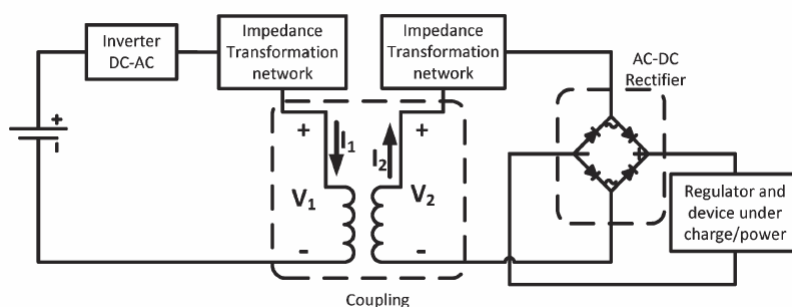


Figure 6.1: Overview of a wireless power transfer system [12]

The input DC voltage first gets changed by an inverter to an AC voltage. Afterwards this AC voltage gets transformed by the air-core transformer to the receiver side of the system and lastly it is transformed back to a DC voltage by a rectifier. The power right after the receiver coil L_2 is given by equation 6.1 [13].

$$P = \frac{\omega I_1^2 M^2}{L_2} \quad (6.1)$$

The formula shows that a high current at the transmitter side I_1 and the mutual inductance M between the transmitter coil L_1 and receiver coil L_2 is important for a high power at the output. Another important design parameter is the maximum efficiency given by equation 6.2 [13].

$$\eta_{max} = \frac{k^2 Q^2}{(1 + \sqrt{1 + k^2 Q^2})^2} \quad (6.2)$$

This means that a high quality factor Q and coupling coefficient k will give a better maximum efficiency.

6.2. Qi

One of the requirements was that the wireless power system has to be designed according to the Qi standard. It follows that the wireless charging receiver should have the following Qi features [14]:

- The system operates at a frequency in the range of 87-205kHz.
- The power is transported using near-field magnetic waves.
- It should have a baseline power delivery of 5W and can have an extended power profile of 15W.
- There is a communication protocol between the transmitter and the receiver to take control of the power transferred.

6.2.1. COMMUNICATION WITH THE TRANSMITTER

One of features Qi has to offer is communication between the transmitter and receiver. The communication consists of four phases shown in figure 6.2: Selection, Ping, Identification & Configuration and Power Transfer. The solid arrows indicate which actions the transmitter undertakes and dashed-dotted arrows indicate the actions which the receiver commences.

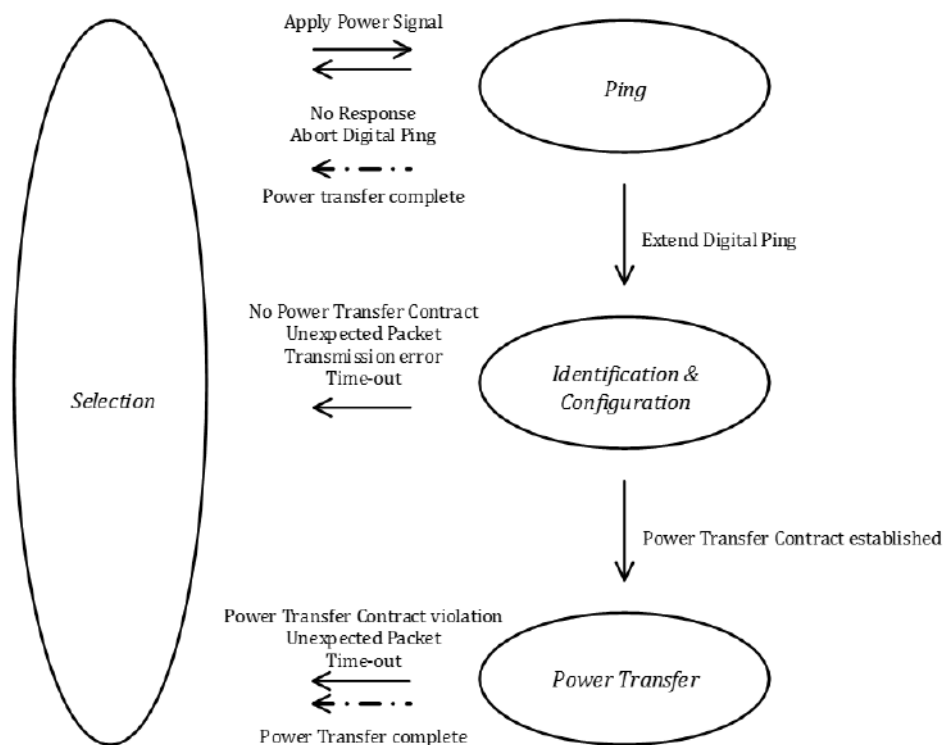


Figure 6.2: The phases of the power transfer at the transmitter and receiver side [14]

SELECTION

This is the phase the receiver starts in. It will measure the rectified voltage and if this value exceeds a certain threshold it will proceed to ping phase. The transmitter will go to the ping phase if it detects a target power receiver. Sometimes it will still go to the ping phase even if the information was insufficient. Nonetheless it will go back to the selection phase if it gets no response back [14].

PING

In this phase the transmitter will send a ping signal. If the transmitter detects a receiver it will continue to send the ping signal and proceeds to the Identification & Configuration phase. If the ping signal does not continue it will go back to the selection phase. The receiver sends a signal strength packet to the transmitter to tell the transmitter to keep the power signal on [15].

IDENTIFICATION & CONFIGURATION

In this phase the receiver sends an identification and configuration packet to the transmitter with information about the maximum power it can receive. From these packets a power transfer contract is created which

contains the boundaries for several parameters for the power transfer. Afterwards it will go to the power transfer phase. If an error happens in this phase it will return to the selection phase [14].

POWER TRANSFER

The transmitter will send power to the receiver according to the information of the configuration packet. The transmitter keeps an eye on the power transfer contract for any violation. If an error happens it will abort the power transfer and go back to the selection. The system also goes back to the selection phase if an end power packet is sent from the receiver to the transmitter [14].

6.3. DESIGN

To include all the Qi features the first choice was the P9221-RAHGI8 wireless power receiver because of its ability to receive 15W of power and because of its high output voltage which would result in less losses in the DC-DC conversion afterwards. It is also convenient that the IC is Qi compliant so it should have all the features from above and already has a rectifier included [16]. However, the IC comes in a package that is connected through a ball grid array with a pitch of 0.4mm of the balls. Because of this, the manufacturer was unable to produce a PCB where this IC could be placed on. To avoid the ball grid array connection the P9025AC IC was chosen afterwards. The IC has almost the same functions as the P9221-RAHGI8 such as communicating with the microcontroller via I²C about its status and enabling and disabling the system. However, it has as only downside that it is only able to deliver 5W [15]. The whole schematic can be seen in appendix A.2. Most of the components from the schematic were chosen according to [15], nonetheless some of the components such as the receiver coil had to be determined.

6.3.1. RECEIVER COIL

For the Qi wireless power receiver a receiver coil is still needed. As seen from equations 6.1 and 6.2 a high mutual inductance and high quality factor are important parameters to maximize the output power and efficiency. A higher mutual inductance will also give a higher coupling coefficient as shown in equation 6.3. This means that a higher mutual inductance will also result in a higher efficiency.

$$M = k\sqrt{L_1L_2} \quad (6.3)$$

DIAMETER OF THE COIL

Another thing to keep in mind are the outer and inner diameter of the receiver coil. The outer diameter is limited to 80mm however this does not impose a problem because it is not practical to use a diameter larger than or almost equal to the outer diameter of the transmitter coil. If the outer diameters of the coils are approximately equal it will be hard to get the coils perfectly aligned. This will result in some losses. With a smaller outer diameter coil it will be ensured that the receiver coil will be completely in the field of the transmitter coil. The exact value of the outer diameter does not matter for the value of the coupling coefficient. The value of the coupling coefficient depends on the ratio between the inner diameter and the outer diameter of the coil. This would be maximized when the outer diameter is three times larger than the inner diameter [17]. Another study showed that if a large coil area is utilized it will have a larger coupling coefficient [18].

SHAPE OF THE COIL

Coils come in different shapes such as circular, rectangular or square which could influence the coupling coefficient. Revealed in [18] was that the actual shape indeed has some effect on the coupling coefficient. The circular coil has a slightly higher coupling coefficient than the rectangular and square shape. The difference in coupling coefficient is relatively small in comparison to the difference of coil area utilized.

RECEIVER COIL CHOICE

With all the parameter considerations given so far in this subsection a receiver coil has to be chosen. If the receiver coil would be made by hand it would lead to higher probability of mistakes in the manufacturing of the coil which will result in lower tolerance parameters such as the inductance and the quality factor. To avoid this problem it was decided to choose for the WR555540-16K2-FS2 with its specifications in table 6.1.

Table 6.1: Specifications of the WR555540-16K2-FS2 receiver coil.

Inductance[μH]	Resistance[Ω]	Quality factor	Inner diameter[mm]	Outer diameter[mm]
15.8	0.10	98.0	19	54

This receiver coil was chosen mainly for its high quality factor, coil area and circular shape.

6.3.2. DUAL RESONANT CIRCUIT

Qi makes use of a dual resonant circuit as shown in figure 6.3. The capacitor C_s has the function to improve the power factor of the circuit and the capacitor C_d enables a resonant detection method [14].

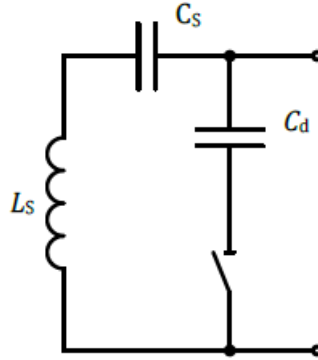


Figure 6.3: Dual resonant circuit[14]

The capacitors C_s and C_d are calculated by equation 6.4 and equation 6.5.

$$C_s = \frac{1}{L'_s(2\pi f_s)^2} \quad (6.4)$$

$$C_d = \frac{1}{L_s(2\pi f_d)^2 - \frac{1}{C_1}} \quad (6.5)$$

Where f_s is 100kHz and f_d is 1MHz. The L_s and L'_s are the self-inductance of the coil without and with magnetically active material close to the coil. To measure L'_s a special shielding material of TDK corp has to be used but this would be too expensive to buy. So for simplicity the same self-inductance is used for L'_s and L_s in equations 6.4 and 6.5. This would approximately give C_s is 150 μ F and C_d is 1.8nF.

7

POWER CONVERSION

There are different kind of DC-DC converters, each having their own advantages and disadvantages. This chapter will mainly be about the Ćuk converter because this is the topology that was chosen. This chapter will explain why this particular topology was picked over the others and how this was implemented in the power system design.

7.1. THEORETICAL BACKGROUND

The Ćuk converter named after Slobodan Ćuk is a DC-DC converter and has an inverting output, just like a buck-boost converter. An advantage of this converter is that the output ripple current of the output is very small in comparison to other topologies because of the two inductors at the input and output [19]. This will result in lower power losses [20] and also reduce EMI problems [21]. Furthermore it is later shown in this section that it is, just like a buck-boost converter, able to convert the output voltage to a higher or lower value than the input voltage. In figure 7.1 the topology of a Ćuk converter is displayed.

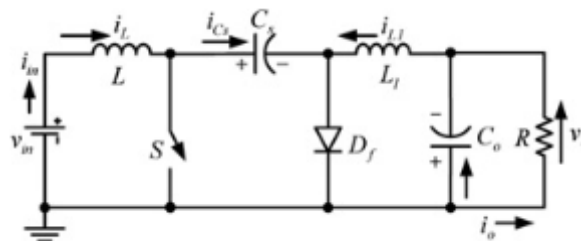


Figure 7.1: A standard Ćuk converter [21]

7.1.1. THE ĆUK CONVERTER IN DIFFERENT STATES

The Ćuk converter is actually a combination of a boost converter followed by a buck converter. The switch S switches to the on or off state with a certain switching frequency. In figures 7.2 and figure 7.3 the different states are shown when the Ćuk converter switch is on or off and its current path is shown for each state.

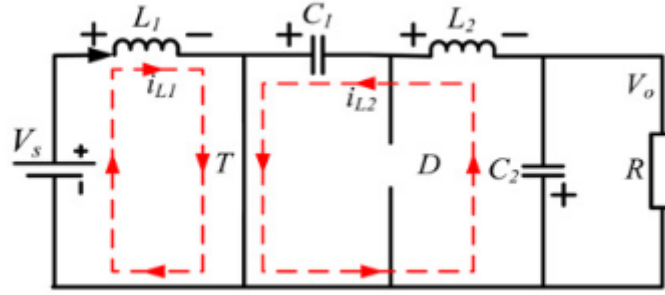


Figure 7.2: Ćuk converter when the switch is on [20]

In the on state the switch becomes a short circuit which results in the fact that energy will be stored in inductor L_1 . Coupling capacitor C_1 will discharge its energy gained in the previous off state to the inductor L_2 , output capacitor C_2 and the load R [20]. Similar to for a buck converter it can be assumed that the ripple voltage at the output is very small because of capacitor C_2 [22]. Using this and Kirchoff's current law the following formula was derived:

$$\Delta V_{C1} = \frac{I_o D T_s}{C_1} \quad (7.1)$$

The ripple of the coupling capacitor depends on the output current I_o , duty cycle D , switching period T_s and coupling capacitor C_1 . The ripple voltage should be kept at a value the capacitor is able to handle.

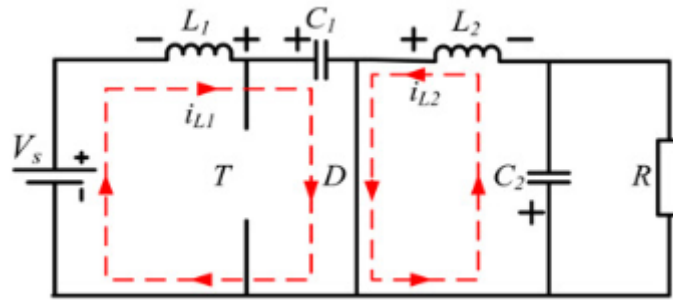


Figure 7.3: Ćuk converter when the switch is off [20]

In the off state the switch becomes an open circuit which will make the L_1 release some energy to C_1 . C_1 charges because of the energy released from L_1 [20]. L_2 releases its energy to C_2 and R . By using Kirchoff's voltage law the following equation can be drafted:

$$\Delta I_L = \frac{V_o(1-D)T_s}{L} \quad (7.2)$$

Here T_s is the switching period, D is the duty cycle, V_o the output voltage and L is the inductance. Equation 7.2 gives the ripple current in the inductor. This can be used for either L_1 or L_2 . The ripple current should preferably be kept at a value which the inductor can still handle, similarly as for the coupling capacitor. The constant switching will result in similar input and output relations as the buck-boost converter:

$$\begin{aligned} \frac{V_o}{V_s} &= -\frac{D}{1-D} \\ \frac{I_s}{I_o} &= -\frac{D}{1-D} \end{aligned} \quad (7.3)$$

So by changing the duty cycle D of the switching frequency the output voltage and current can be changed to its desired value. The output voltage ripple is given by [23]:

$$\Delta V_o = \Delta I_{L2} \left(ESR_{C2} + \frac{1}{8f_s C_2} \right) \quad (7.4)$$

The ripple is dependent on the ripple current from L_2 , the equivalent series resistor of the output capacitor C_2 , the switching frequency and the capacitance of C_2 .

7.2. DESIGN

The input interfaces need to be converted to a variable output voltage between the 12-16.8V. To do this the schematic in appendix A.3 was designed. The schematic consists of a power path controller and two Ćuk converters. One of the Ćuk converter is controlled by an LT1370 and the other one makes use of MOSFET using a PWM with MPPT control from the microcontroller.

7.2.1. POWER PATH CONTROLLER

It is difficult to imagine a situation where one would want to charge the batteries using the laptop charger and the wireless charger at the same time. For this reason the choice was made to use only a single DC/DC converter for both charging interfaces. This brings the advantage of a cost and space reduction due to less components being needed compared to using separate converters. To realize this, a circuit is needed that connects either the laptop charger or the wireless charging receiver to the DC/DC converter, depending on which charger is in place. As the laptop charger can charge the battery at a much higher rate than the wireless charger, it was chosen to connect the laptop charger in case for some reason both chargers are present. These design choices lead to the following requirements for the circuit:

- In case only one charger is in place, connect this charger to the DC/DC converter.
- In case both chargers are in place, connect the laptop charger to the DC/DC converter.
- In case no chargers are available, disconnect both the laptop charger and the wireless charging receiver.

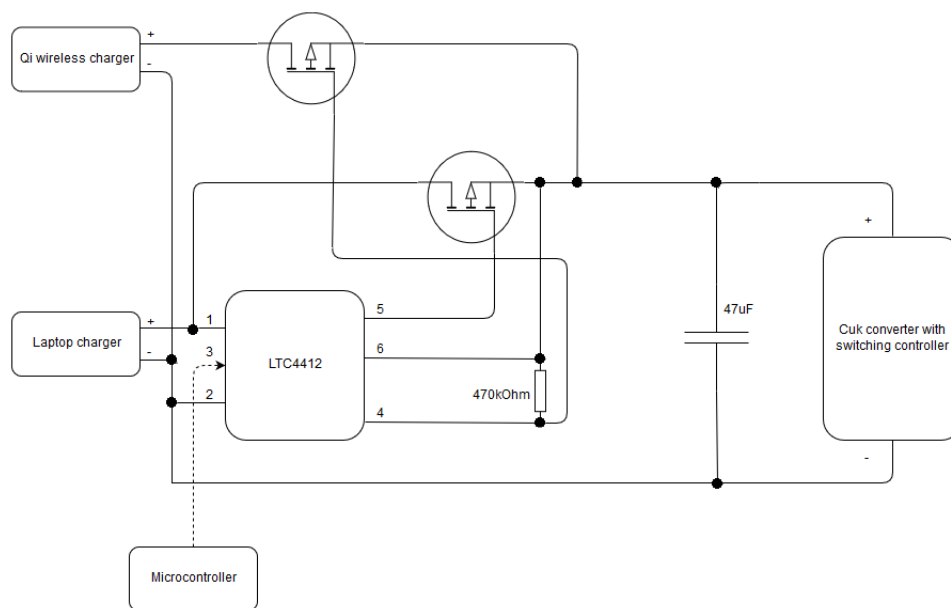


Figure 7.4: The LTC4412 power path controller

The power path controller makes use of an LTC4412. This is shown in figure 7.4. A more detailed schematic can be found in appendix A.3. The IC is connected to two p-channel MOSFETs which will be switched on or off depending on the input of the LTC4412. The LTC4412 compares pin 1 and pin 6 to see which of the two inputs has a higher voltage. With pin 5 the IC switches the MOSFET of the laptop charger on or off and with pin 4 it switches the MOSFET of the Qi charger on or off depending on the cases as given earlier in this section [24]. At the end of the power path controller a capacitor was placed to prevent voltage spikes when a charger is being connected.

7.2.2. ĆUK CONVERTER OF THE LAPTOP AND QI INPUT

The power path controller is connected to a Ćuk converter using an LT1370 switching regulator. A simplified schematic is displayed in figure 7.5 and a more detailed schematic can be seen in appendix A.3. The IC offers output voltage control using a resistor divider. The internal switch in the LT1370 is turned on or off by a gate driver which is connected to an oscillator controlled by pin 6. It constantly gets feedback from from this pin so it is able to change its duty cycle accordingly [25]. Pin 5 and pin 4 serve a similar role as the drain and source of a MOSFET. The output voltage is given by [25]:

$$V_{out} = -2.48 \left(1 + \frac{R_1}{R_2} \right) + I_{NFB} R_1 \quad (7.5)$$

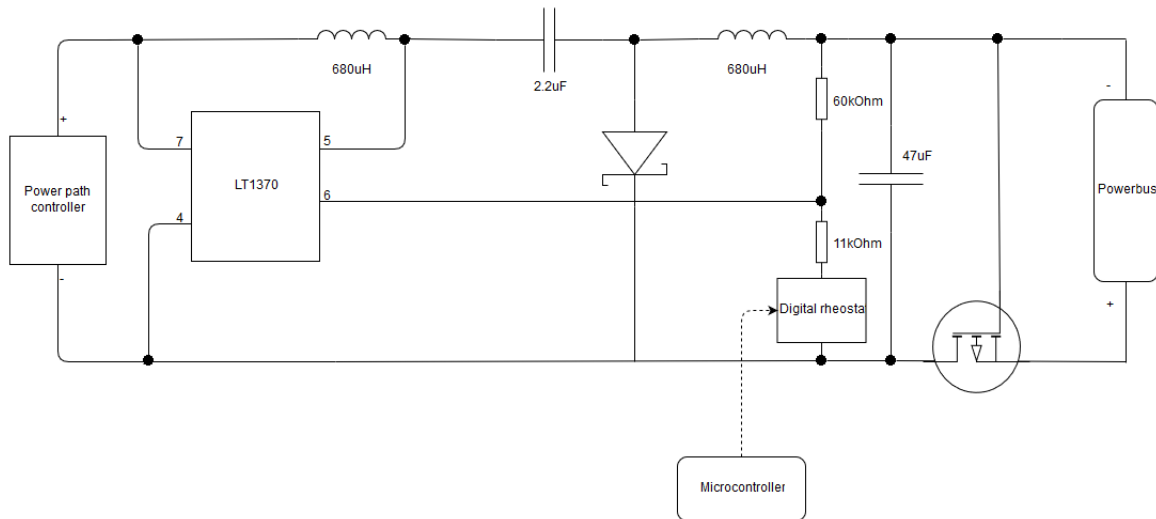


Figure 7.5: The Ćuk converter with switching regulator

The bias current I_{NFB} is $30\mu A$. The resistor R_1 is the upper resistor and resistor R_2 is the bottom resistor. The output voltage of the converter needs to match the voltage of the power bus. Because this voltage can vary from 12V-16.8V, a variable output voltage is needed. This was implemented using a digital rheostat. The maximum value of this rheostat is $10k\Omega$ and the resistance can be changed via an I²C connection with the microcontroller. Using equation 7.5, R_1 and R_2 need to be set, so that the output voltage can range from 12V to 16.8V. This was achieved by replacing R_2 with a digital rheostat with a resistance ranging from 0 to $10k\Omega$ in series with an $11k\Omega$ resistor. For R_1 a $60k\Omega$ resistor was used, these values were chosen because they allowed us to set the output voltage with the best resolution. This was found by writing a MATLAB script that shows the step size that the output voltage can be set with. Figure 7.6 shows the resolution of the output voltage over the relevant output voltage range and shows a resolution of at least 80mV.

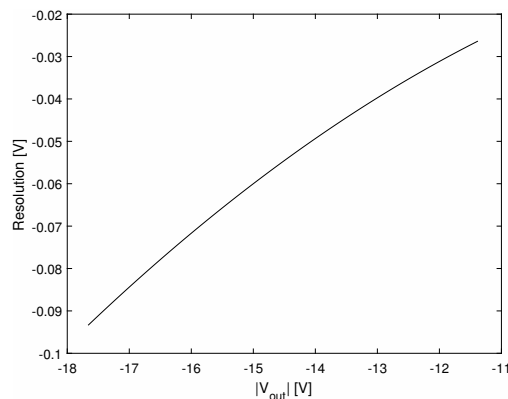


Figure 7.6: The resolution that the output voltage can be set with using a digital rheostat in resistor divider.

The values for the coupling capacitor and inductors were estimated using equations 7.1 and 7.2. As the switching frequency is 500kHz and the coupling capacitor is $2.2\mu\text{F}$, this results in a ripple voltage of 1.91V. With an inductor of $680\mu\text{H}$ this would give a ripple current of 0.011A. The output capacitance was calculated using equation 7.4 which would give with a $47\mu\text{F}$ capacitor with an ESR of $150\text{m}\Omega$ an output ripple voltage of 1.7mV.

7.2.3. ĆUK CONVERTER OF THE SOLAR MODULE

For the solar module an n-channel MOSFET is used instead of a switching controller to allow the implementation of an MPPT algorithm to control the duty cycle. It is important that the gate-source voltage is low because of the 3.3V peak voltage of the PWM from the microcontroller. So a MOSFET with a gate-source voltage of 0.55V was chosen. At the input of the converter an INA226 sensor is placed that measures the power of the solar module. The measurements will be used for the MPPT algorithm as described in chapter 5.

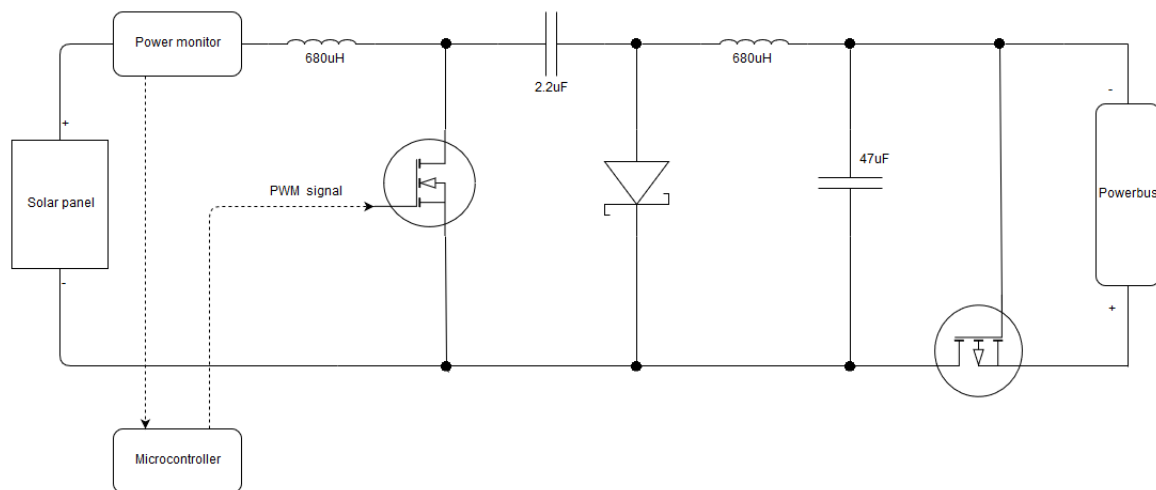


Figure 7.7: The Ćuk converter of the solar module

The values for the coupling capacitor and inductors were calculated using equations 7.1 and 7.2. As the frequency of the PWM from the microcontroller is 20kHz and the coupling capacitor is $2.2\mu\text{F}$ this would give a ripple voltage of 2.49V. With an inductor of $680\mu\text{H}$ this would result in a ripple current of 0.33A. The output capacitance was calculated using equation 7.4. Using a $47\mu\text{F}$ capacitor with an ESR of $150\text{m}\Omega$ the output ripple voltage will be 0.092V.

7.2.4. SAFETY

At the end of both converters blocking p-type MOSFETs are placed. This is to protect the input interfaces in case the system gets incorrectly connected. Because these MOSFETs will usually be either on or off for long durations, the switching losses of these MOSFET are insignificant. Thus, the dominant losses of these MOSFETs are caused by their on resistance (R_{DS-ON}). To reduce the losses, MOSFETs with an R_{DS-ON} of only $5.3\text{m}\Omega$ were chosen for the blocking mosfets.

Another safety measure taken was installing fuses at the input of the DC/DC converters. The fuses blow when the current exceeds the maximum current that can be handled by the converters, which is 5A for the laptop charger and wireless receiver Ćuk converter and 1A for the solar panel Ćuk converter. These fuses protect the system when chargers that deliver too much current are connected.

8

TESTING AND RESULTS

After designing the system, it is important to verify that the system works according to expectations. For this reason, all of the subsystems needed to be tested:

- The solar panel
- The Ćuk converter belonging to the solar panel
- The wireless charging module
- The power path selector
- The Ćuk converter belonging to the wireless charging module and the laptop charger.

For all of these subsystems test setups were made, except for the wireless charging module. The wireless charging module initially consisted of the P9221-RAHG18, a wireless power receiver IC, that needs to be connected to the circuit via a ball grid array connection. With the tools available to make a prototype, it was not possible for us to connect this chip to make a test setup with the initial chip. As stated in chapter 6, a different wireless power receiver IC was chosen later. A test setup to test the wireless charging module with this chip could have been made, but at the time of the change, not enough time was available to effectuate this. Due to issues with finances of TU Delft, the PCB of the complete power management system has not been received yet. Because of this, our whole system has not been built at the time of this writing yet and has therefore also not been tested. This chapter discusses the test setups that have been built, the measurements that were carried out with these setups and a cost analysis.

8.1. SOLAR PANEL

A series of measurements was carried out to find the actual performance and parameters of the solar panel. The P-V curve of the solar panel was determined. This shows the power output of the solar panel for every solar panel voltage. A solar simulator was used to simulate the solar light incident on the panel. The conditions from this solar simulator used were a bit different than the STC:

- The temperature during measurements was 61.5 °C instead of 25 °C.
- The light irradiance was 850 W/m² instead of 1000 W/m².

A rheostat was used to vary the ratio between the voltage and the current at the load. The solar panel voltage and current were measured using multimeters. This resulted in the P-V curve that can be seen in figure 8.1.

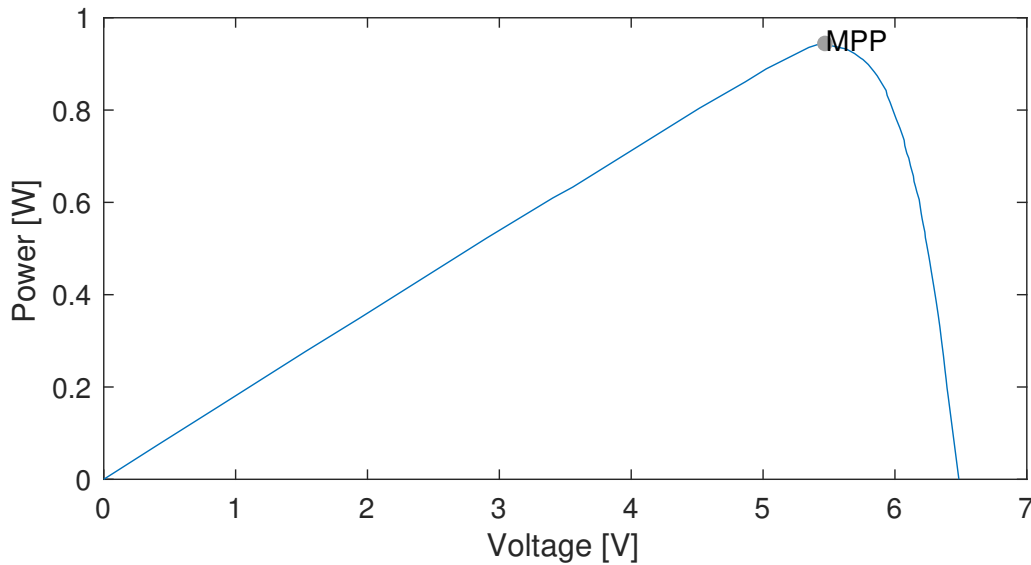


Figure 8.1: Power-Voltage curve of the system's solar panel where the grey dot denotes the maximum power point of the solar panel.

From the plot it becomes clear that the 2.5 W power output specified by the manufacturer is not achieved. This can be partly attributed from the test conditions being different from the STC that solar panel manufacturers use to test their panels. To begin, the light irradiance during our test was 15% lower, meaning that 15% less solar energy was available at the panel's surface. Additionally, the performance of a solar panel suffers from temperature increases. For poly-Si, for every 1°C of temperature increase, the solar cell efficiency goes down by 0.4% [26]. In our case, this leads to an efficiency drop of 14.6% due to the higher temperature.

8.2. ĆUK CONVERTER OF THE SOLAR PANEL

The DC/DC converter of the solar panel meets its requirements if it can increase the PV voltage (typically 6V) to the power bus voltage (12V-16.8V). A prototype of the converter was built to find out if this was the case. The converter was tested by connecting 6V 0.4A power source to its input. These values were chosen as they are the typical operating voltage and current of the solar panel according to the specifications from the manufacturer. The gate of the MOSFET was driven by a function generator that delivered a PWM signal with a high voltage level of 3.3V, a low voltage level of 0V and a frequency of 100kHz. Using the function generator, a duty cycle sweep was done to find out to what range of power bus voltages the converter can step up the voltage. The measurement results are plotted in figure 8.2.

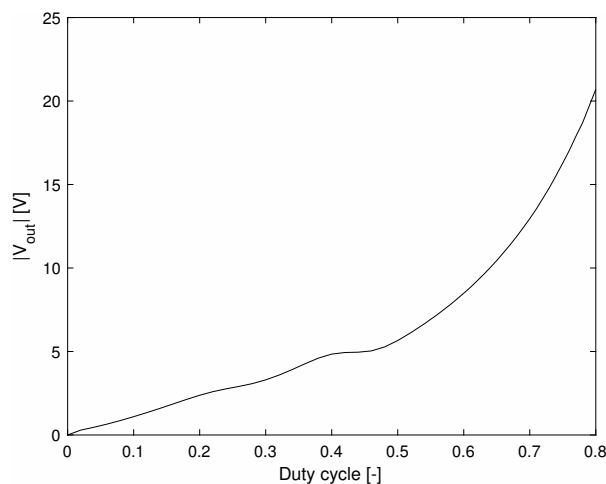


Figure 8.2: Measurements of the output voltage of the Ćuk converter for the solar panel for the range of duty cycles from 0 to 0.8.

As can be seen in the figure, the Ćuk converter output voltage can cover the whole range of power bus voltage levels. As an additional test, small changes were made to the voltage at the input and the powerbus voltage of 12V-16.8V was still within the range. This enables the microcontroller to generate a PWM signal and implement an MPPT method by altering the duty cycle of this PWM signal. However, problems occurred when the control subgroup was testing the Ćuk converter using a PWM signal coming from the microcontroller. It seemed like the microcontroller could not deliver enough power to turn on the MOSFET fast enough. This could be fixed in the final design, where a different MOSFET will be used with a smaller threshold voltage that will allow the microcontroller to turn it on faster. In case this also does not work, the alternative of using a gate driver circuit that is controlled by the microcontroller was proposed.

8.3. POWER PATH SELECTOR

To test the functionality of the power path selector, a prototype of the circuit was made and two voltage sources were connected to the inputs of the power path selector: An 18V source to simulate a laptop charger being connected and a 5V source to simulate a wireless charging pad being positioned under the wireless receiver module. Figure 7.4 shows an overview of the setup used to test the power path selector circuit.

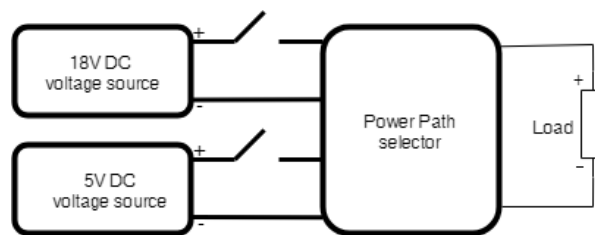


Figure 8.3: Setup to test the properties of the power path selector circuit.

The voltage sources were switched on and off in such ways to consider all possible cases of the charging devices being present or absent. The results of this test can be found in table 8.1. From the table it becomes apparent that if one of the voltage sources is connected to the power path selector, the selector connects this source to the load and if both of the sources are connected, only the laptop charger will be connected to the load.

Table 8.1: The possible input states of the power path selector.

18V source	5V source	Load voltage
OFF	OFF	0V
OFF	ON	5V
ON	OFF	18V
ON	ON	18V

8.4. ĆUK CONVERTER OF THE WIRELESS CHARGING MODULE AND THE LAPTOP CHARGER

Finally, the DC/DC converter used for the laptop charger and the wireless charging module needed to be tested. A prototype of the converter was made, with two differences compared to the final schematic as discussed in chapter 7:

- The digital rheostat was not included in the voltage divider circuit. Instead, a regular resistor was used to test the functionality.
- The resistors of the voltage divider circuit had larger tolerances (5%) and a larger temperature coefficients (100 ppm/°C)

During the tests, it was found that the circuit stepped up the voltage that we applied at the input, but not by the desired amount. The resistors used were $R_1 = 10 \text{ k}\Omega$ and $R_2 = 2.2 \text{ k}\Omega$. Following the equation specified in the datasheet [25] of the LT1370 voltage regulator, a voltage of -13.7V should be present at the output. However, an output voltage of only -7.0V was measured. Nonetheless, some success was found in the sense

that by installing different resistors in the voltage divider circuit, the output voltage was increased. From this it can be concluded that controlling the output voltage using a digital rheostat is possible to a certain extent. Further investigation of the prototype was planned, but unfortunately the LT1370 voltage regulator broke down before this was possible. The resistors and digital rheostat that will be used in the final design are far less tolerant and less dependent on temperature. This should enable us to set the output voltage of the Ćuk converter more precisely. However, due to the LT1370 breaking down, it is unsure at this moment that the output voltage can be set with the accuracy required for correct operation.

8.5. COST ANALYSIS

As was specified in chapter 2, a requirement was that costs of the whole power management system and battery management system should not be more than €100 per robot. This section first shows the total costs of making a single prototype of the system. Because the robot needs to be semi-mass produced, most of the costs per component drop when they are purchased in large quantities. For this reason, the total costs are also shown when the components are purchased for 150 robots at once.

8.5.1. PROTOTYPE

In table 8.2 the price of the whole system is specified per part. The total price for a single prototype is €283.30. As can be seen a large part of this comes from the PCB price. The components contribute to about half of the total costs.

Table 8.2: The price of the system-parts for a single prototype [27]

Part	Amount	Cost [€]
Batteries	8	38.40
Main PCB	1	31.00
BMS PCB	1	42.00
Components main PCB	1	134.47
Components BMS PCB	1	24.84
Coil	1	9.59
Solar Panel	1	3.00

8.5.2. SEMI-MASS PRODUCTION

In table 8.3 the price of the system is specified per part. The total price of a series of 150 is estimated to be €17435.18. For this analysis, the components price was estimated based on an average discount for a series of 150. This comes down to €116.23 per robot. This is a bit more than the maximum costs specified in chapter 2. However, the requirement can still be met if the project proposer prefers a system containing only 4 batteries. This would bring down the costs to about €100, with the drawback that the robot will be able to store less energy in the batteries. Another option is to look for cheaper alternative solutions for parts of the PMS or the BMS.

Table 8.3: The price of the system-parts for semi-mass production [27]

Part	Amount	Cost [€]
Batteries	1200	3,720.00
Main PCB	150	230.60
BMS PCB	150	241.83
Components main PCB	150	10,085.25
Components BMS PCB	150	1,863.00
Coil	150	919.50
Solar Panel	150	375.00

9

CONCLUSION AND RECOMMENDATIONS

The goal of this project was to develop the input conversion of a power management system from the DeciZebro. The system has three input interfaces: a laptop charger, a wireless power transfer module and a solar module.

9.1. DESIGN PROCESS

The design process started by finding a solar panel and receiver coil for the Qi wireless power transfer system. Poly-Si solar cells were used because of their low price, high efficiency and availability on the market. The solar panel has an operating voltage of 6V which makes it easier to convert to the desired voltage. For the receiver coil it was important to find one with a high quality factor, coil area and circular shape. The power conversion was done using a Ćuk converter due to smaller ripples at the output than other topologies and the ability to either buck or boost the input voltage. To save some space on the PCB a power path controller was used for the laptop and Qi interface.

9.2. EVALUATION OF SUB-SYSTEMS

Several sub-systems were tested to see if they would be able to function accordingly. The power path selector and Ćuk converter of the solar module worked according to the expectations. However the solar panel was not able to deliver specified output power that was given by the manufacturer. This was partly caused by the high temperature and the lower irradiance conditions during the tests. The Ćuk converter for the laptop charger and Qi wireless power transfer did not meet the intended output voltage. This might have been because of the less tolerant resistors.

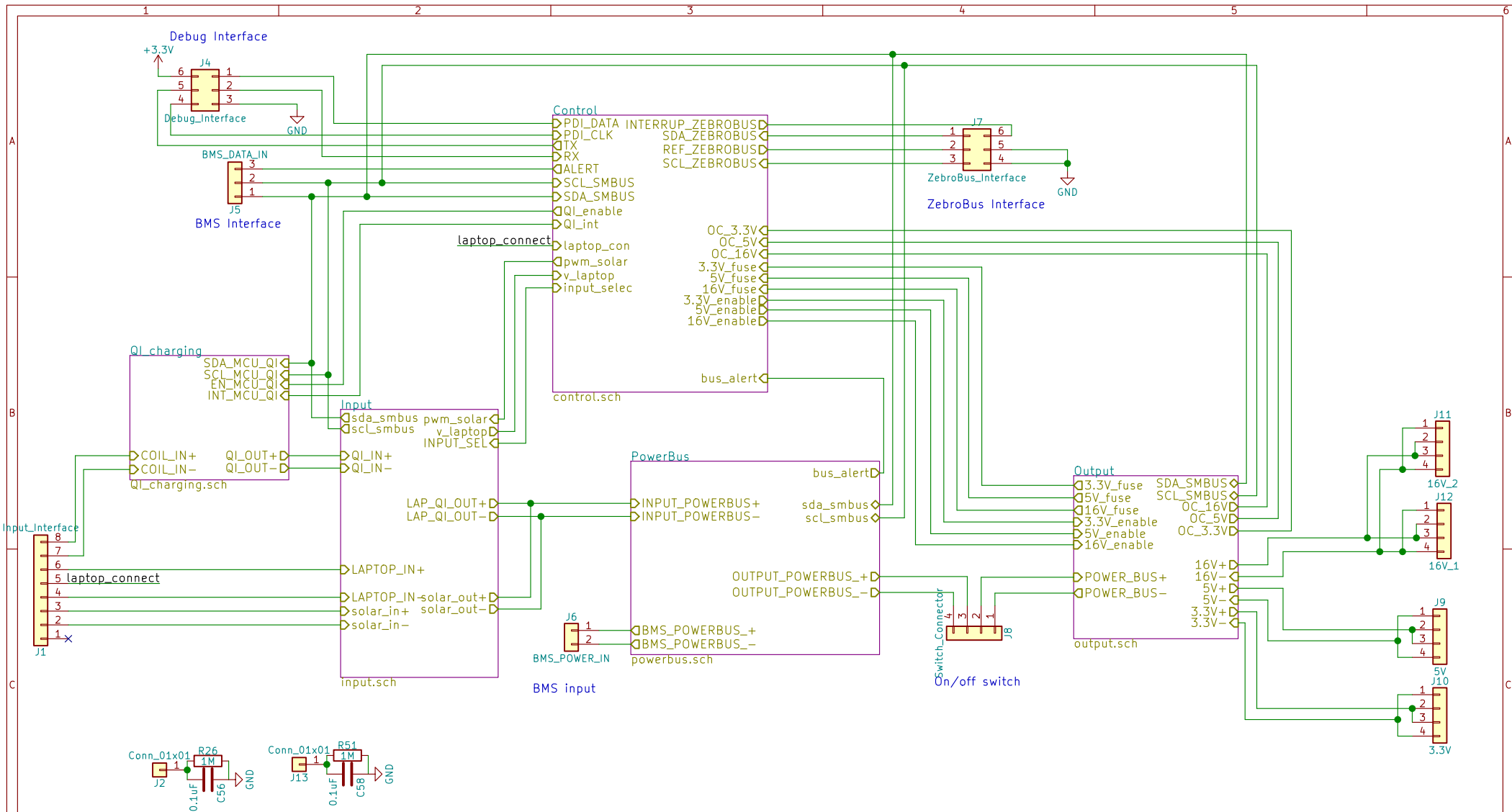
9.3. FUTURE WORK AND RECOMMENDATIONS

The complete power management system with battery management system still has to be tested with all sub-modules. This means that it is possible to further test certain sub-modules as for example the Ćuk converter of the laptop charger and Qi wireless power transfer. In the case this would still not function as desired then it would be possible to replace the switching controller with an n-channel MOSFET controlled by a gate driver. With the main PCB it will be possible to test the Ćuk converter of the solar module with the MPPT algorithm. It is also possible to test with a higher frequency of 170kHz from the microcontroller PWM. In case the problem where the microcontroller is unable to turn on the n-channel MOSFET of the solar Ćuk converter reoccurs, this must be fixed by installing a gate driver circuit for this MOSFET. Some improvements could be made by reducing the inductor values of the Ćuk converter, so less space is required on the main PCB.

A

SCHEMATICS AND DRAWING

A.1. MAIN

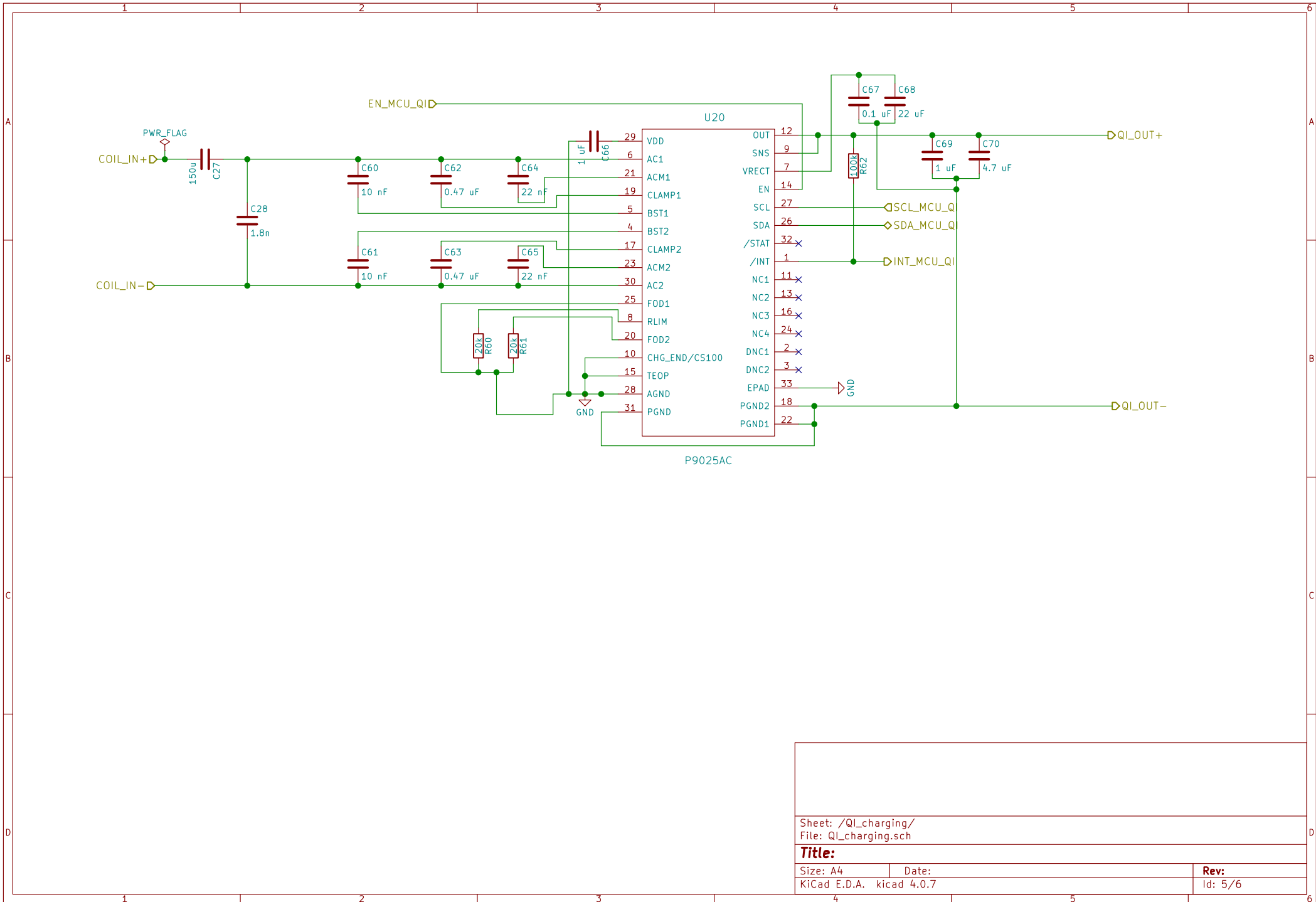


Sheet: /
 File: main.sch

Title:

Size: A4	Date:	Rev:
KiCad E.D.A. kicad 4.0.7		Id: 1/6

A.2. WIRELESS POWER TRANSFER



Sheet: /Qi_charging/
 File: Qi_charging.sch

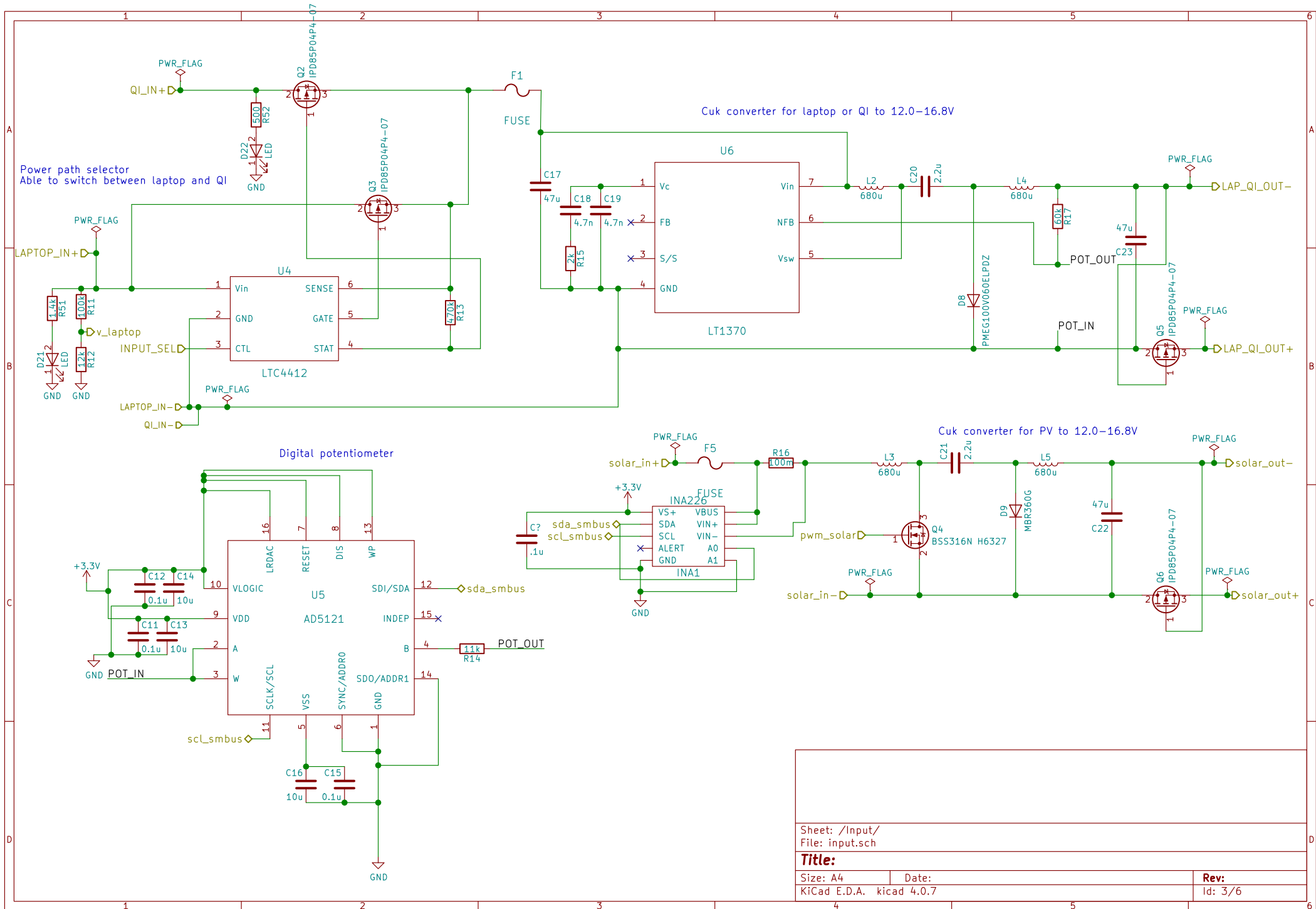
Title:

Size: A4
 KiCad E.D.A. kicad 4.0.7

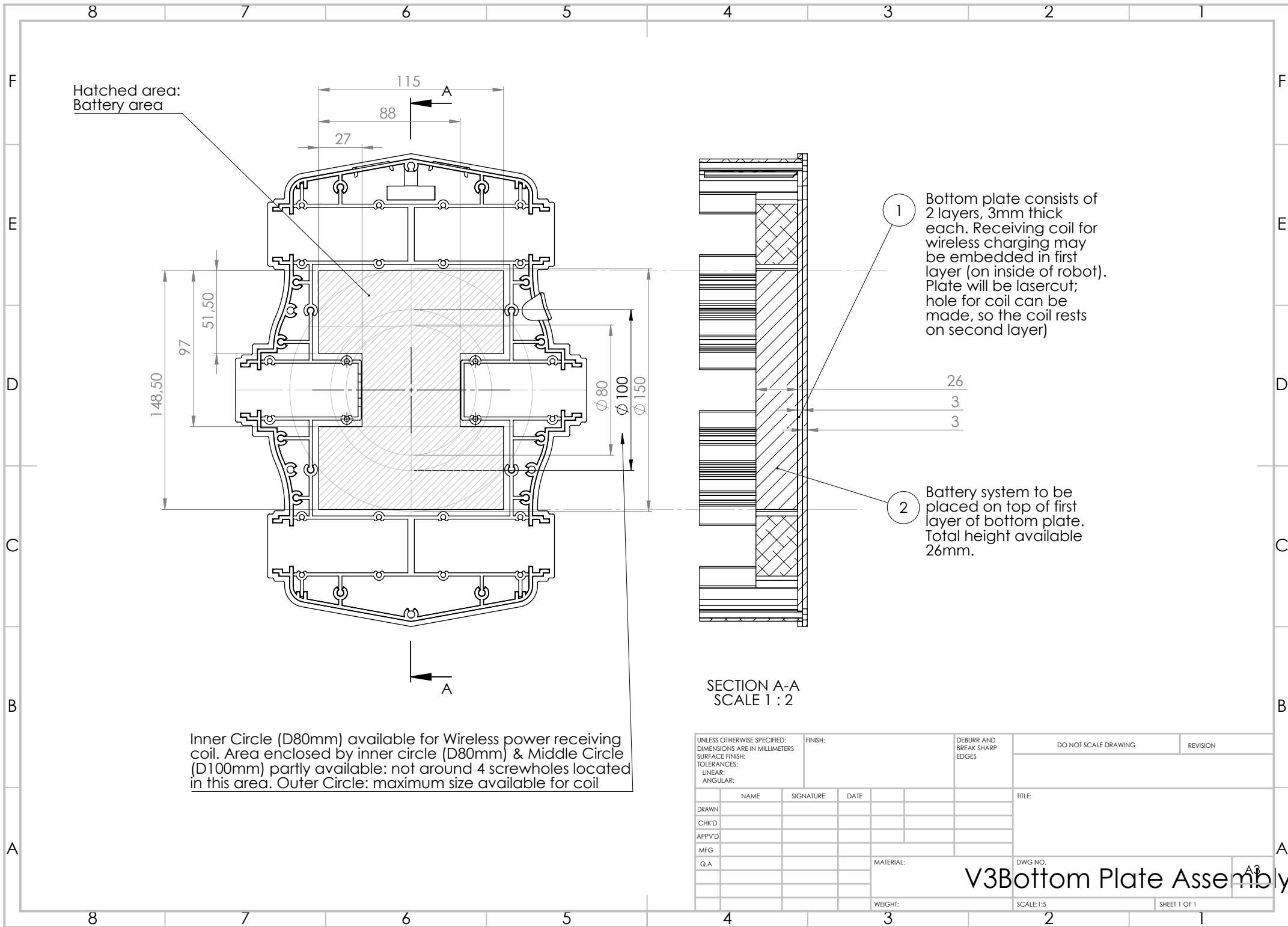
Date:

Rev:
 Id: 5/6

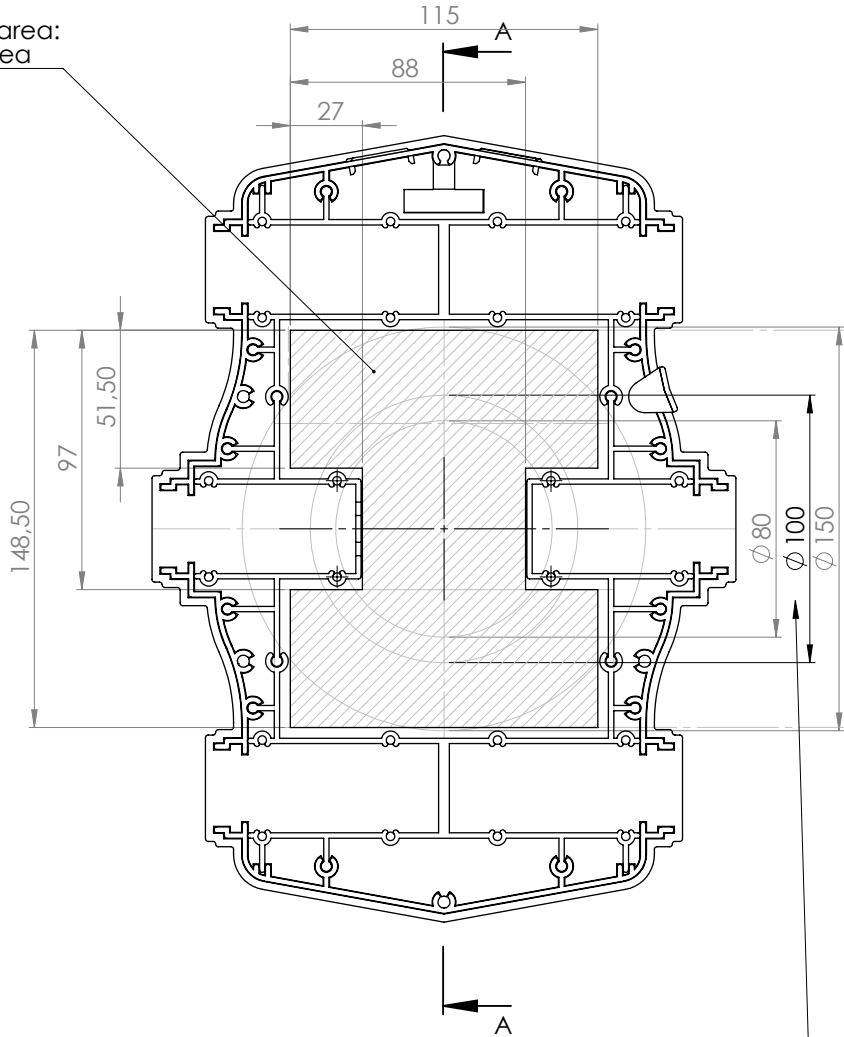
A.3. POWER CONVERSION



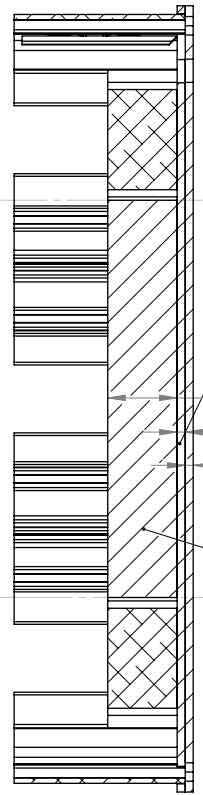
A.4. DRAWING OF THE DECIZEBRO



Hatched area:
Battery area



Inner Circle (D80mm) available for Wireless power receiving coil. Area enclosed by inner circle (D80mm) & Middle Circle (D100mm) partly available: not around 4 screwholes located in this area. Outer Circle: maximum size available for coil



1 Bottom plate consists of 2 layers, 3mm thick each. Receiving coil for wireless charging may be embedded in first layer (on inside of robot). Plate will be lasercut; hole for coil can be made, so the coil rests on second layer)

26
3
3

2 Battery system to be placed on top of first layer of bottom plate. Total height available 26mm.

SECTION A-A
SCALE 1 : 2

UNLESS OTHERWISE SPECIFIED: DIMENSIONS ARE IN MILLIMETERS		FINISH:		DEBURR AND BREAK SHARP EDGES		DO NOT SCALE DRAWING		REVISION	
SURFACE FINISH:									
TOLERANCES:									
LINEAR:									
ANGULAR:									
NAME	SIGNATURE	DATE				TITLE:			
DRAWN									
CHK'D									
APPV'D									
MFG									
Q.A									
					MATERIAL:	DWG NO.		A3	
					WEIGHT:	SCALE:1:5		SHEET 1 OF 1	

V3Bottom Plate Assembly

B

DERIVATIONS OF THE RIPPLE CURRENT OF THE INDUCTORS AND RIPPLE VOLTAGE OF THE COUPLING CAPACITOR FROM A ĆUK CONVERTER

B.1. RIPPLE VOLTAGE OF THE COUPLING CAPACITOR

By making the assumption that the ripple voltage of the load R is very small the following relationship is derived:

$$C \frac{\Delta V_{C1}}{\Delta t} = I_o \quad (\text{B.1})$$

Δt is the time in which the circuit is in the on state.

$$\Delta t = DT_s \quad (\text{B.2})$$

So this will give:

$$\Delta V_{C1} = \frac{I_o DT_s}{C_1} \quad (\text{B.3})$$

B.2. RIPPLE CURRENT OF THE INDUCTORS

For L_2 the following formula follows from Kirchhoff's voltage law:

$$L_2 \frac{\Delta I_{L2}}{\Delta t} = V_o \quad (\text{B.4})$$

Δt is the time in which the circuit is in the off state.

$$\Delta t = (1 - D)T_s \quad (\text{B.5})$$

So this results in:

$$\Delta I_{L2} = \frac{V_o(1 - D)T_s}{L_2} \quad (\text{B.6})$$

For L_1 the following formula follows from Kirchhoff's voltage law:

$$L_1 \frac{\Delta I_{L1}}{\Delta t} + V_s = V_o + V_s \quad (\text{B.7})$$

Δt is the time in which the circuit is in the off state.

$$\Delta t = (1 - D)T_s \quad (\text{B.8})$$

So this results in:

$$\Delta I_{L1} = \frac{V_o(1 - D)T_s}{L_1} \quad (\text{B.9})$$

BIBLIOGRAPHY

- [1] M. Green, K. Emery, Y. Hishikawa, W. Warta, and E. Dunlop, *Solar cell efficiency tables (version 48)*, in *Progress in Photovoltaics: Research and Applications*, Vol. 24 (2016) pp. 905–913.
- [2] N. Tanaka, *Technology roadmap: solar photovoltaic energy*, (2010).
- [3] J. Dawidziuk, *Review and comparison of high efficiency high power boost dc/dc converters for photovoltaic applications*, *Bulletin of the Polish Academy of Sciences: Technical Sciences*, **59** (2011).
- [4] K. Jäger, O. Isabella, A. Smets, R. van Swaaij, and M. Zeman, *Solar Energy Fundamentals, Technology, and Systems* (Delft University of Technology, Delft, 2014).
- [5] J. Ahmad, *A fractional open circuit voltage based maximum power point tracker for photovoltaic arrays*, in *2010 2nd International Conference on Software Technology and Engineering*, Vol. 1 (2010) pp. V1–247–V1–250.
- [6] H. Matsuo and F. Kurokawa, *New solar cell power supply system using a boost type bidirectional dc-dc converter*, *IEEE Transactions on Industrial Electronics* **IE-31**, 51 (1984).
- [7] T. Noguchi, S. Togashi, and R. Nakamoto, *Short-current pulse-based maximum-power-point tracking method for multiple photovoltaic-and-converter module system*, *IEEE Transactions on Industrial Electronics* **49**, 217 (2002).
- [8] J. J. Nedumgatt, K. B. Jayakrishnan, S. Umashankar, D. Vijayakumar, and D. P. Kothari, *Perturb and observe mppt algorithm for solar pv systems-modeling and simulation*, in *2011 Annual IEEE India Conference* (2011) pp. 1–6.
- [9] N. Femia, G. Petrone, G. Spagnuolo, and M. Vitelli, *Optimization of perturb and observe maximum power point tracking method*, *IEEE Transactions on Power Electronics* **20**, 963 (2005).
- [10] M. Kaouane, A. Boukhelifa, and A. Cheriti, *Implementation of incremental-conductance mppt algorithm in a photovoltaic conversion system based on dc-dc zeta converter*, in *2016 8th International Conference on Modelling, Identification and Control (ICMIC)* (2016) pp. 612–617.
- [11] L. de Jong and N. Fakkkel, *Development of power system control for the decizebro*, (2018).
- [12] Z. N. Low, R. A. Chinga, R. Tseng, and J. Lin, *Design and test of a high-power high-efficiency loosely coupled planar wireless power transfer system*, *IEEE Transactions on Industrial Electronics* **56**, 1801 (2009).
- [13] S. Chatterjee, A. Iyer, C. Bharatiraja, I. Vaghasia, and V. Rajesh, *Design optimisation for an efficient wireless power transfer system for electric vehicles*, *Energy Procedia* **117**, 1015 (2017), first International Conference on Power Engineering Computing and CONTROL (PECCON-2017) 2nd -4th March .2017. Organized by School of Electrical Engineering, VIT University, Chennai, Tamil Nadu, India.
- [14] Qi wireless power consortium, *Introduction to the power class 0 specification*, (2018), retrieved June 15, 2018 from: <https://www.wirelesspowerconsortium.com/developers/specification.html>.
- [15] IDT, *P9025ac datasheet qi wireless power receiver with integrated rectifier and ldo output*, (2015), retrieved June 15, 2018 from: <https://www.idt.com/document/dst/p9025ac-datasheet>.
- [16] IDT, *P9221-r datasheet wireless power receiver for 15w applications*, (2017), retrieved June 15, 2018 from: <https://www.idt.com/document/dst/p9221-r-datasheet>.
- [17] T. Seshimo, T. Yamamoto, and K. Koshiji, *Downsizing of coreless coils for transcutaneous energy transmission in implantable devices - improvement of coupling factor and efficiency between coils*, in *2013 35th Annual International Conference of the IEEE Engineering in Medicine and Biology Society (EMBC)* (2013) pp. 1871–1874.

- [18] R. Bosshard, J. Mühlethaler, J. W. Kolar, and I. Stevanović, *Optimized magnetic design for inductive power transfer coils*, in *2013 Twenty-Eighth Annual IEEE Applied Power Electronics Conference and Exposition (APEC)* (2013) pp. 1812–1819.
- [19] S. Cuk and R. D. Middlebrook, *A new optimum topology switching dc-to-dc converter*, in *1977 IEEE Power Electronics Specialists Conference* (1977) pp. 160–179.
- [20] Z. Sun and Z. Yang, *Improved maximum power point tracking algorithm with cuk converter for pv systems*, *The Journal of Engineering* **2017**, 1676 (2017).
- [21] M. Zhu and F. L. Luo, *Voltage-lift-type cuk converters: topology and analysis*, *IET Power Electronics* **2**, 178 (2009).
- [22] B. Ferreira and W. van der Merwe, *The principles of electronic and electromechanic power conversion a system approach* (John Wiley & Sons, Hoboken, NJ, 2014).
- [23] Linear Technology, *Lt8330-low iq boost/sepic/inverting converter with 1a, 60v switch*, (2015), retrieved June 16, 2018 from: <http://www.analog.com/media/en/technical-documentation/data-sheets/8330fa.pdf>.
- [24] Linear Technology, *Ltc4412-low loss powerpath controller in thinsot*, (2002), retrieved June 16, 2018 from: <http://www.analog.com/media/en/technical-documentation/data-sheets/4412fb.pdf>.
- [25] Analog Devices, *Lt1370 datasheet 500khz high efficiency 6a switching regulator*, (2014), retrieved June 16, 2018 from: <http://www.analog.com/en/products/power-management/switching-regulators/sepic-regulators/lt1370.html>.
- [26] E. Skoplaki and J. Palyvos, *On the temperature dependence of photovoltaic module electrical performance: A review of efficiency/power correlations*, *Solar Energy* **83**, 614 (2009).
- [27] F. van Veelen and W. Lopes, *Development of a battery management system and output for the decizebro*, (2018).